

Static and Dynamic Structures of InBr_x ($x = 1.4, 1.5, 1.75, \text{ and } 2$) Studied by ^{81}Br NQR and ^{115}In NMR

Koji Yamada, Hiroshi Mohara, Tomotaka Kubo, Takashi Imanaka, Kazue Iwaki,
Hiroshi Ohki, and Tsutomu Okuda

Graduate School of Science, Hiroshima University,
Kagamiyama 1-3, 739-8526 Higashi-Hiroshima, Japan

Reprint requests to Dr. K. Y.; E-mail: kyamada@sci.hiroshima-u.ac.jp

Z. Naturforsch. **57 a**, 375–380 (2002); received April 2, 2002

Presented at the XVIth International Symposium on Nuclear Quadrupole Interactions,
Hiroshima, Japan, September 9-14, 2001.

Structure and bonding properties of InBr_x (In_5Br_7 , In_2Br_3 , In_4Br_7 and InBr_2) were studied by ^{81}Br and ^{115}In NQR, and ^{115}In NMR. The ethane-like $[\text{Br}_3\text{In}^{\text{II}}-\text{In}^{\text{II}}\text{Br}_3]^{2-}$ anion was confirmed in In_5Br_7 or In_2Br_3 by ^{81}Br NQR and the anion was characterized by the high quadrupole coupling constant at the ^{115}In site ($e^2Qq/h \approx 350$ MHz). On the other hand, In_4Br_7 showed successive phase transitions and was characterized as $[\text{In}^{\text{I}}]_5[\text{In}^{\text{III}}\text{Br}_4]_2[\text{In}^{\text{III}}\text{Br}_6]$ by means of ^{81}Br NQR and ^{115}In NMR below 370 K. A disordered structure at the cationic sublattice was supposed at Phase I above 370 K. NMR signals assigned to the In^{I} could not be detected for the powdered sample, however, all quadrupole coupling constants (e^2Qq/h) and chemical shifts (σ_{iso}) could be determined using a single crystal. The In^{I} sites show relatively large e^2Qq/h and also show larger distribution of the chemical shift suggesting a diversity of the In^{I} coordination similar to the isoelectronic main group elements such as Sn^{II} or Sb^{III} .

Key words: ^{115}In NMR; Single Crystal; Quadrupole Coupling Constant; Phase Transition.

1. Introduction

The chemistry of indium halocomplexes is interesting for three reasons: 1) The three oxidation states of indium, In^{I} , In^{II} , and In^{III} lead to an interesting structural variety. 2) In^{II} is expected to appear as the result of dynamical mixing of In^{I} and In^{III} . 3) Halocomplexes of indium, such as in Li_3InBr_6 [1 - 3] and Li_3InCl_6 [4], may be cation superconductors.

The crystalline compounds between InBr and InBr_2 ($= \text{In}^{\text{I}}[\text{In}^{\text{III}}\text{Br}_4]$) [5] are In_5Br_7 ($\text{InBr}_{1.4}$) [6 - 8], In_2Br_3 ($\text{InBr}_{1.5}$) [9], and In_4Br_7 ($\text{InBr}_{1.75}$) [10]. These crystals are more appropriately formulated as $[\text{In}^{\text{I}}]_3[\text{In}^{\text{II}}_2\text{Br}_6]\text{Br}$, $[\text{In}^{\text{I}}]_2[\text{In}^{\text{II}}_2\text{Br}_6]$, and $[\text{In}^{\text{I}}]_5-[\text{In}^{\text{III}}\text{Br}_4]_2[\text{In}^{\text{III}}\text{Br}_6]$, respectively. $[\text{Br}_3\text{In}-\text{InBr}_3]^{2-}$, Br^- , InBr_4^- , and InBr_6^{3-} form anionic sublattices for the counter cations In^+ . We have synthesized and characterized these compounds by means of powder X-ray diffraction, DTA, ^{81}Br and ^{115}In NQR, and ^{115}In NMR. In this paper we mainly discuss the bonding, structure and phase transitions of In_4Br_7 because of its structural changes with temperature.

2. Experimental

All compounds were synthesized from In metal and InBr_3 , which was purified by sublimation. For each compound a stoichiometric mixture of In and InBr_3 was heated in an evacuated sealed tube at 350 °C for three days, and the homogeneous mixture was quenched to room temperature and annealed for a week just below the melting point. Single crystals of In_4Br_7 and InBr_2 were also obtained from the melt by the Bridgman technique. All samples were characterized by XRD measurements.

^{81}Br and ^{115}In NQR was obtained with a conventional pulsed spectrometer. The assignment of the ^{81}Br and ^{79}Br NQR signals was confirmed by the quadrupole moment ratio $Q(^{79}\text{Br})/Q(^{81}\text{Br}) = 1.1971$. ^{115}In NMR was carried out with a similar spectrometer at 6.4 T. An acidic solution of $\text{In}(\text{NO}_3)_3$ was used as chemical shift standard. A home made variable temperature NMR probe with a goniometer was used to observe the angular dependence of the ^{115}In NMR.

Table 1. ^{81}Br NQR frequencies of In_5Br_7 , In_2Br_3 , In_4Br_7 , and InBr_2 at 77 K.

Compound	Chemical Formula	^{81}Br NQR Frequency / MHz	Assignment
In_5Br_7	$(\text{In}^+)_3(\text{In}_2\text{Br}_6^{2-})(\text{Br}^-)$	88.665 ^a , 87.921, 87.711, 86.663, 85.792, 82.197, 80.444, 79.994, 79.515, 71.324, 71.011	$[\text{Br}_3\text{In-InBr}_3]^{2-}$
In_2Br_3	$(\text{In}^+)_2(\text{In}_2\text{Br}_6^{2-})$	90.309, 88.989, 82.753, 80.438, 78.139, 72.245, 71.185	$[\text{Br}_3\text{In-InBr}_3]^{2-}$
In_4Br_7	$(\text{In}^+)_5(\text{InBr}_4^-)_2(\text{InBr}_6^{3-})$	110.05, 107.93, 107.42, 107.06, 106.87, 104.48, 103.48 ^a , 103.04, 102.40, 102.13, 101.25 ^a , 99.09, 98.99, 97.00	InBr_4^-
		58.49, 58.16, 57.97, 57.16, 57.04, 56.26, 55.93, 55.02, 54.73, 54.18, 53.10, 51.59	InBr_6^{3-}
InBr_2	$(\text{In}^+)(\text{InBr}_4^-)$	106.479, 104.055	InBr_4^-

^a Doublet

Compd.	Method	<i>T</i> /K	^{115}In NQR freq. / MHz				e^2Qq/h^{-1} /MHz	η	σ_{iso} /ppm	Assignment
			ν_1	ν_2	ν_3	ν_4				
In_5Br_7	NQR	77	27.97	26.44	41.96	56.58	343.4	0.413	$[\text{Br}_3\text{In-InBr}_3]^{2-}$	
			28.22	26.64	42.58	57.18	346.5	0.414		
			28.51	27.04	42.87	57.97	351.2	0.411		
			29.01	27.20	43.58	58.26	353.3	0.418		
In_4Br_7	NMR	298					6.50	0.0	$\text{In}^{\text{III}}(1), \text{InBr}_4^-$	
							1.85	0.0	$\text{In}^{\text{III}}(2), \text{InBr}_6^{3-}$	
							61.5	0.0	$\text{In}^{\text{I}}(3), \text{In}^+$	
							41.4	0.0	$\text{In}^{\text{I}}(4), \text{In}^+$	
							22.9	0.0	$\text{In}^{\text{I}}(5), \text{In}^+$	
InBr_2	SEDOR	77	1.761	1.162	1.214	1.811	11.93	0.956	InBr_4^-	
	NMR	298					12.8	0.93	InBr_4^-	

Table 2. ^{115}In NQR and NMR Parameters for In_5Br_7 , In_4Br_7 , and InBr_2 .^a Estimated from the single crystal data at 230 K.

3. Results and Discussion

3.1. ^{81}Br and ^{115}In NQR parameters for In_5Br_7 , In_2Br_3 , In_4Br_7 , and InBr_2

Table 1 summarizes the ^{81}Br ($I = 3/2$) NQR frequencies for In_5Br_7 , In_2Br_3 , In_4Br_7 and InBr_2 . The ^{81}Br NQR frequencies were divided into the three groups 100 - 110 MHz, 70 - 90 MHz and 51 - 59 MHz, and these groups could be assigned to InBr_4^- , $[\text{Br}_3\text{In-InBr}_3]^{2-}$ and InBr_6^{3-} anions, respectively. Table 2 summarizes the ^{115}In ($I = 9/2$) NQR and NMR parameters determined by several different techniques. The ^{115}In NQR spectrum for In_5Br_7 , assigned to the four crystallographically different $[\text{Br}_3\text{In-InBr}_3]^{2-}$ anions, was consistent with the structure [9]. Although a large e^2Qq/h parameter (348.6 MHz on average) was expected for the In-In bond, the asymmetry parameter of ca. 41% was much higher than expected. This large asymmetry parameter may suggest strong interactions between the anions and In^+ cations.

Two ^{81}Br NQR signals were observed for InBr_2 continuously from 77 K to 298 K with the same intensity ratio, suggesting a C_{2v} - $mm2$ point symmetry

of the InBr_4^- anion. As Table 2 shows, all four ^{115}In NQR transitions were detected by means of spin-echo double resonance (^{81}Br NQR \leftrightarrow ^{115}In NQR) at 77 K. The small e^2Qq/h with a large asymmetry parameter is consistent with the point symmetry of the InBr_4^- anion. This assignment was also confirmed by the second-order quadrupole effect of the ^{115}In NMR at 298 K, as will be discussed later. However, a ^{115}In NMR signal assigned to the In^{I} site could not be detected due to its large e^2Qq/h .

3.2. Successive Phase Transitions of In_4Br_7 Detected by DTA and ^{81}Br NQR

The representative DTA of In_4Br_7 is shown in Fig. 1 together with the phases determined by DTA, X-ray diffraction, and ^{81}Br NQR. This compound shows four phase transitions at 95, 195, 280, and 370 K and melts at ca. 460 K. The phase transitions at 95 K and 370 K showed hysteresis in the NQR and DTA. A complicated situation arises by the fact that the crystal from the melt is metastable. Although the crystalline sample obtained from the melt is more stable than its powder state, it changes to a white powder after several weeks. Furthermore, a mechanical stress such as

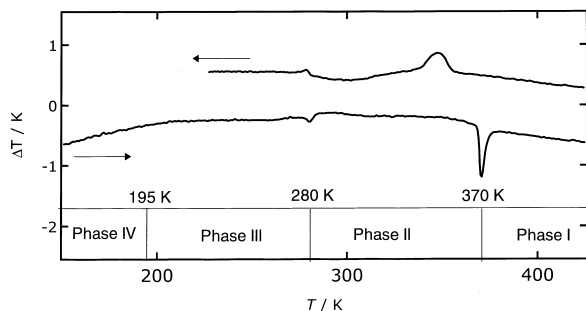


Fig. 1. DTA heating and cooling curves for In_4Br_7 together with the phases.

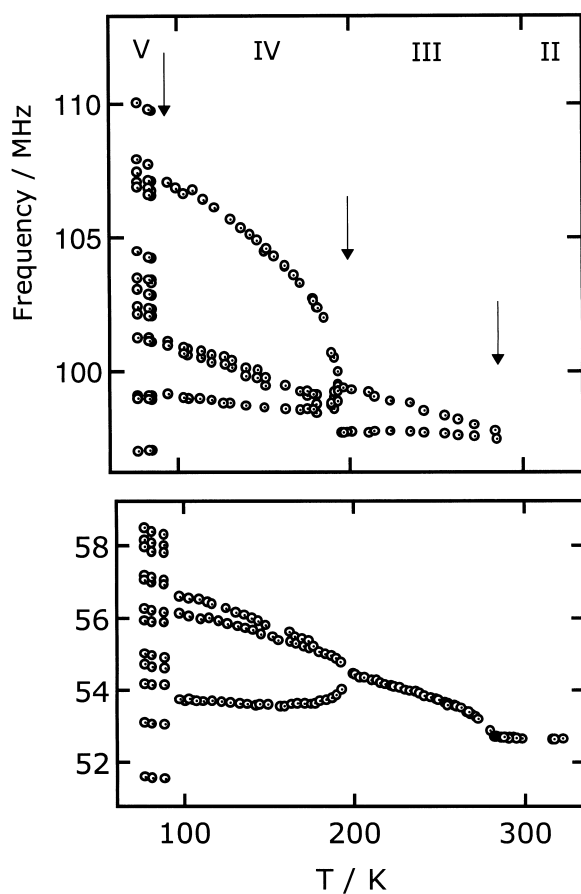


Fig. 2. Temperature dependence of ^{81}Br NQR for In_4Br_7 . Two frequency regions assigned to InBr_4^{3-} and InBr_6^{3-} anions are shown separately.

grinding accelerates this phase transition and showed a quite different XRD pattern which could be indexed as an orthorhombic system with $a = 747.3$ pm, $b = 1056.1$ pm, and $c = 1439.1$ pm. On heating again

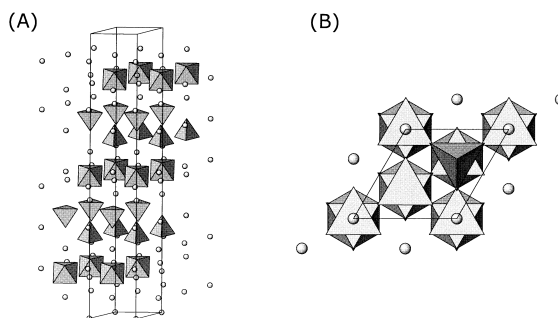


Fig. 3. Crystal structure of the trigonal In_4Br_7 , $a = 757.75$ pm, $c = 4657.7$ pm with $R\bar{3}m$ [10]. Small circles indicate In^+ cations. (A) Drawing perpendicular to the c -axis and (B) parallel to the c -axis.

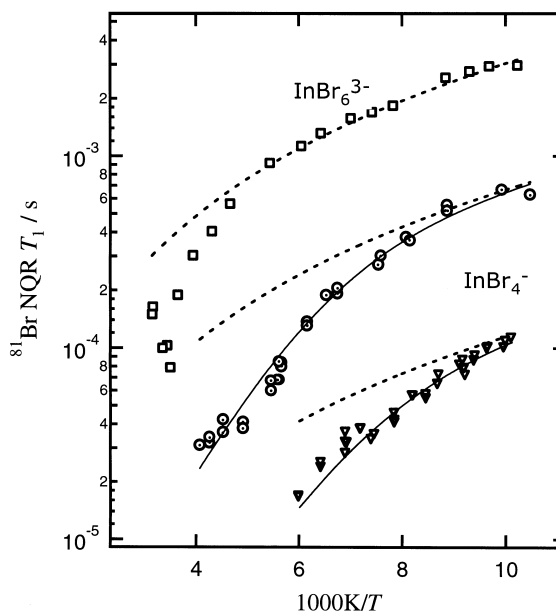


Fig. 4. Temperature dependence of ^{81}Br NQR T_1 for In_4Br_7 . The dotted lines denote the Raman process, $1/T_1 = \alpha T^2$.

above 420 K, this powder pattern changed to the original trigonal phase and could be maintained down to room temperature.

Figure 2 shows the temperature dependence of the ^{81}Br NQR which appears in two different regions. Although some signals overlapped each other at 77 K, sixteen and twelve ^{81}Br NQR signals could be detected for the tetrahedral InBr_4^- and the octahedral InBr_6^{3-} anions, respectively. This finding suggests that there are four crystallographically different tetrahedral anions and two octahedral anions, and this result is consistent with the formula $[\text{In}^{\text{I}}]_5[\text{In}^{\text{III}}\text{Br}_4]_2-$

$[\text{In}^{\text{III}}\text{Br}_6]$. At ca. 95 K the number of the ^{81}Br NQR lines decreased to four and three discontinuously, and further two and one above 195 K for the tetrahedral and octahedral site, respectively. The point symmetry of the InBr_4^- anion in Phase III is C_{3v} - $3m$, because this phase shows two ^{81}Br NQR signals with intensity ratio 1:3 from the high frequency side. On the other hand, the InBr_6^{3-} anion shows only one ^{81}Br NQR signal, suggesting a D_{3h} - $\bar{3}m$ point symmetry. Figure 3 shows the structure of In_4Br_7 reported by Dronskowski. Our NQR results at Phase II and III are consistent with the structure. As Fig. 2 shows, the NQR signals assigned to InBr_4^- anion disappeared at ca. 280 K accompanied by a gradual decrease of the spin-lattice relaxation time T_1 . Therefore T_1 was observed as a function of temperature as shown in Fig. 4, where the dotted lines correspond to the Raman process ($1/T_1 = aT^2$). Except for an anomalous behavior near $T_{\text{tr}} = 280$ K, the T_1 vs. $1/T$ curve assigned to the InBr_6^{3-} anion obeys the Raman process. On the other hand, T_1 vs. $1/T$ plots assigned to the InBr_4^- anion deviate from the Raman process and are expressed by the equations

$$1/T_1 = 0.869 \text{ s}^{-1}\text{K}^{-2} \cdot T^2 + 1.45 \cdot 10^7 \text{ s}^{-1} \cdot \exp(-8.03 \text{ kJmol}^{-1}/RT), \quad (1)$$

$$1/T_1 = 0.150 \text{ s}^{-1}\text{K}^{-2} \cdot T^2 + 2.81 \cdot 10^6 \text{ s}^{-1} \cdot \exp(-9.05 \text{ kJmol}^{-1}/RT), \quad (2)$$

where the second term represents a contribution from an ionic motion. These activation energies ($E_a = 8 \sim 9 \text{ kJmol}^{-1}$) are too small for a reorientation of the InBr_4^- anion and furthermore, the pre-exponential factors are smaller by several orders than expected. These findings suggested a modulation effect due to some motion of the neighboring cation. One of the possible activation processes is a local motion of the $\text{In}^{\text{I}}(5)$, because it forms the shortest interactions with the InBr_4^- anions and also shows a large temperature dependence of the e^2Qq/h . With decreasing temperature, the $\text{In}^{\text{I}}(5)$ is supposed to shift from the center of the octahedral hole to an off-center position similar to $\text{In}^{\text{I}}(3)$ or $\text{In}^{\text{I}}(4)$. The coordination property of In^{I} will be described later.

3.3. Dynamic Structural Changes Detected by ^{115}In NMR Using Polycrystalline In_4Br_7

Figure 5 shows the temperature dependence of the ^{115}In NMR of polycrystalline In_4Br_7 . At 77 K, two

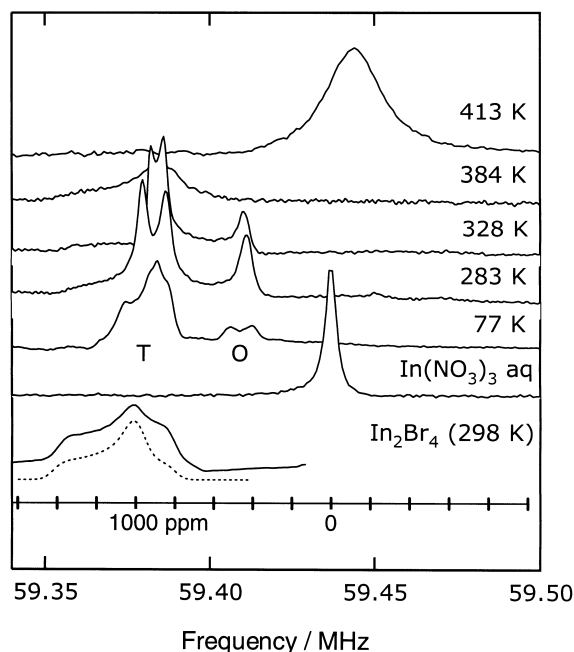


Fig. 5. Temperature dependence of the ^{115}In NMR spectra using a powder sample. A powder pattern of InBr_2 is shown together with a simulation.

well resolved peaks having second order quadrupole effects were observed at around 59.38 MHz (930 ppm) and 59.41 MHz (420 ppm). Low and high frequency peaks could be assigned to the tetrahedral and the octahedral In^{III} sites, respectively, referring to that of the InBr_4^- anion in InBr_2 . Since there are crystallographically four tetrahedral and two octahedral anions at 77 K, only averaged parameters were estimated as $e^2Qq/h = 10.0$ MHz with $\eta = 0.60$ for the tetrahedral site and $e^2Qq/h = 9.0$ MHz with $\eta = 0.0$ for the octahedral site.

Since the crystal undergoes a phase transition to a trigonal system at 195 K, the tetrahedral site shows a typical second order effect with $\eta = 0$. On the other hand, no second order effect was observed for the octahedral site. With further increasing the temperature, the ^{115}In NMR changed drastically at 370 K, at which a strong endothermic peak was observed on the DTA curve. Although the Rietveld refinement above 370 K did not finish, the powder pattern was quite similar to that at 298 K except a change in the intensity. These measurements from NMR, DTA and X-ray suggest that an order-disorder transition takes place in the cationic sublattice at 370 K. A new broad peak appeared around -120 ppm at 413 K, probably

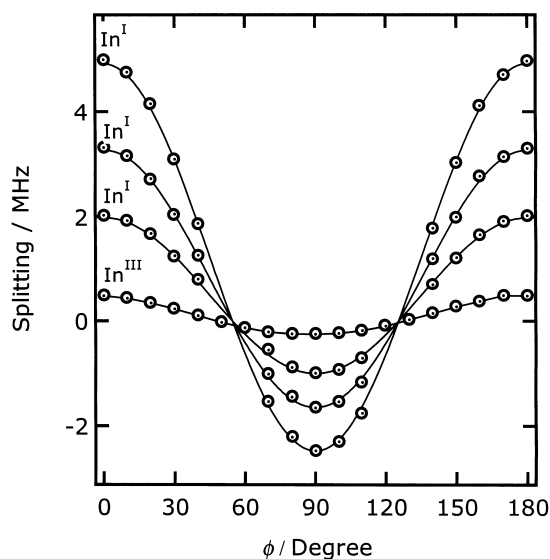


Fig. 6. Angular dependence of the single crystal ¹¹⁵In NMR. The splitting between a pair of the first satellite transitions is plotted against ϕ at 298 K.

as a result of the averaged structure due to cationic diffusion. However, in this stage the oxidation state and the possible positions of the In atoms can not be decided unambiguously only from the NMR.

3.4. Quadrupole Coupling Constants at the In^I and In^{III} Sites by Single Crystal NMR

Using a single crystal, we could determine e^2Qq/h for all In sites. ¹¹⁵In has a nuclear spin $I = 9/2$. Hence 9 allowed transitions ($\Delta m = 1$) are expected for each In site. It was convenient that all In sites are located on the three-fold axis, and hence all q_{zz} directions must be parallel to the c -axis of the trigonal system. Therefore the axially symmetric e^2Qq/h and chemical shift tensor can be determined unambiguously from the rotation pattern about one axis. According to Abragam, the first order quadrupole effect with axial symmetry is expressed as [11]

$$\Delta\nu = \nu_q \cdot (3\cos^2\phi\sin^2\theta - 1), \quad (3)$$

where $\Delta\nu$ means a splitting between a pair of satellite transitions ($1/2 \leftrightarrow 3/2$ and $-1/2 \leftrightarrow -3/2$), $\nu_q = e^2Qqh^{-1}/24$, ϕ an angle of the sample rotation, and θ an angle between q_{zz} and the rotation axis of the crystal. Contributions from the second order quadrupole effect and the chemical shift are canceled out in (3). On the other hand, the contribution from the second order quadrupole effect on the central transition ($-1/2$

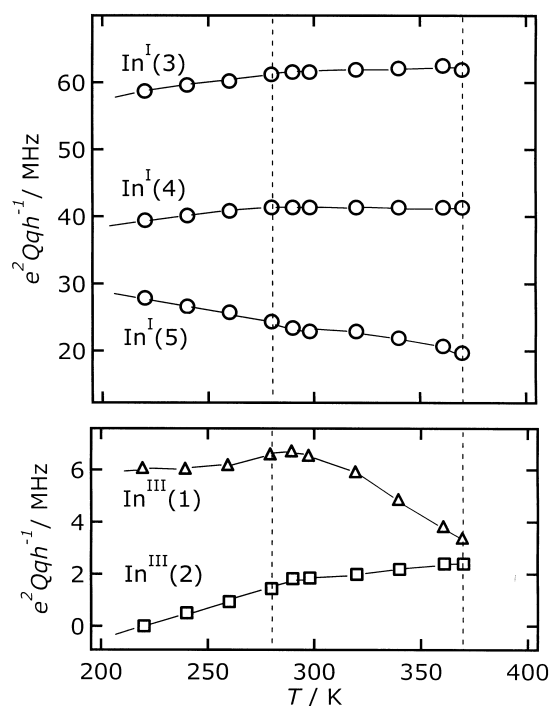


Fig. 7. Temperature dependence of the e^2Qq/h at the five ¹¹⁵In sites. In^{III} (1) and In^{III} (2) sites are assigned to the tetrahedral and octahedral anions, respectively. In^I (3), In^I (4), and In^I (5) are assigned to the In⁺ cations.

$\leftrightarrow 1/2$) is expressed as

$$\nu_{1/2} - \nu_L = (-\nu_q^2/16\nu_L) \cdot (I(I+1) - 3/4) \cdot (1 - \cos^2\phi\sin^2\theta) \cdot (9\cos^2\phi\sin^2\theta - 1), \quad (4)$$

where $\nu_{1/2}$ means an NMR frequency of the central transition with a second order effect, and ν_L a Larmor frequency.

Figure 6 plots the first order splitting as a function of ϕ at 298 K for three In^I sites and a tetrahedral In^{III} site. From this measurement, θ was determined to be 86(1)°. Table 2 summarizes e^2Qq/h parameters for these sites. Furthermore, the temperature dependence of e^2Qq/h could be easily determined from the spectra at an orientation with a maximum splitting ($\phi = 0$). The plot e^2Qq/h vs. T shows a slight change at 280 K as displayed in Figure 7. However, at 370 K (Phase II \leftrightarrow Phase I) all satellite transitions disappeared, suggesting a drastic change of the cationic sublattice. Although the spectrum near ν_L was very complicated, the second order shifts of all central transitions could be traced at 230 K, referring to the first order splittings. From the numerical analysis of the

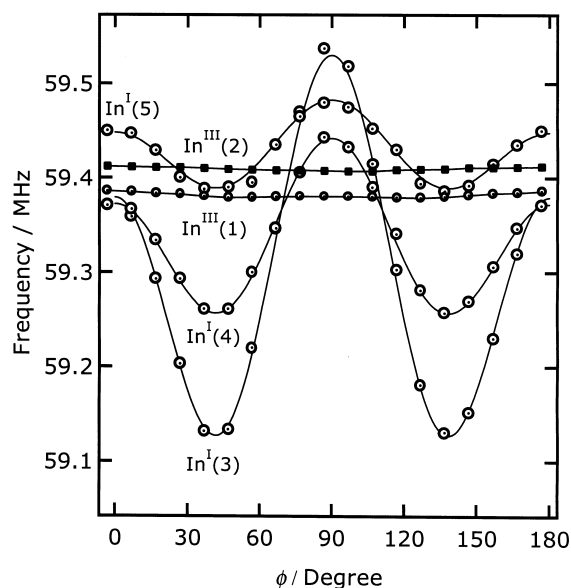


Fig. 8. Angular dependence of the central transitions ($-1/2 \leftrightarrow 1/2$) corresponding to the five In sites at 230 K.

angular dependence shown in Fig. 8, the both e^2Qq/h and chemical shifts (σ_{iso}) were determined. As Table 2 shows, σ_{iso} for the In^{I} sites distribute over 1200 ppm, suggesting a characteristic distortion of the In^{I} coordination. Figure 9 shows the nearest environments of

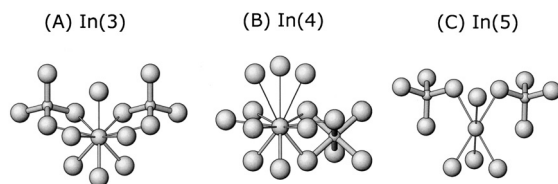


Fig. 9. Coordination around the In^{I} site. (A) Three short In^{I} -Br bond at 327.6 pm. (B) Three short In^{I} -Br bonds at 337.6 pm. (C) Six equivalent In^{I} -Br bonds at 350.6 pm.

the three In^{I} sites. $\text{In}^{\text{I}}(5)$, which showed the smallest e^2Qq/h , was unambiguously assigned to an In at $3a$ (0,0,0) site, shown in Fig. 9(C), because of the roughly half intensity of the ^{115}In NMR compared to the others. This site has a point symmetry $\bar{3}m$ with six bonds at 350.6 pm. On the other hand, $\text{In}^{\text{I}}(3)$ with the largest e^2Qq/h was tentatively assigned to an In^{I} at a $6c$ (0,0,0.4174) site because this In has three short In-Br bonds (327.6 pm) with a considerably distorted coordination. It is especially interesting that the distortion appearing on the In^{I} is quite similar to that observed for the isoelectronic Sn^{II} or Sb^{III} having an s-electron lone pair. This effect has been theoretically studied as a second-order Jahn-Teller instability [10]. However, it is also possible to understand this feature as the hypervalent nature of the main group elements having an s-electron lone pair [12, 13].

- [1] Y. Tomita, H. Ohki, K. Yamada, and T. Okuda, *Solid State Ionic* **136-137**, 351 (2000).
- [2] Y. Tomita, A. Fujii, H. Ohki, K. Yamada, and T. Okuda, *Chem. Lett.* **1998**, 223.
- [3] Y. Tomita, K. Yamada, H. Ohki, and T. Okuda, *Z. Naturforsch.* **53a**, 466 (1998).
- [4] H. J. Steiner and H. D. Lutz, *Z. Anorg. Allg. Chem.* **613**, 26 (1992).
- [5] J. E. Davis, L. G. Waterwarth, and I. J. Worrall, *J. Inorg. Nucl. Chem.* **36**, 805 (1974).
- [6] T. Staffel and G. Meyer, *Z. Anorg. Allg. Chem.* **563**, 27 (1988).
- [7] R. E. Marsh and G. Meyer, *Z. Anorg. Allg. Chem.* **582**, 128 (1990).
- [8] M. Ruck and H. Barnighausen, *Z. Anorg. Allg. Chem.* **625**, 577 (1999).
- [9] T. Staffel and G. Meyer, *Z. Anorg. Allg. Chem.* **552**, 113 (1987).
- [10] R. Dronskowski, *Angew. Chem. Int. Ed. Engl.* **34**, 1126 (1995).
- [11] A. Abragam, *Principles of Nuclear Magnetism*, Oxford University Press, London 1961, Chapt. 7
- [12] K. Yamada and T. Okuda, *Chemistry of Hypervalent Compounds*, ed. by K. Akiba, Wiley-VCH, New York 1999, Chapt. 3.
- [13] K. Yamada, S. Nose, T. Umehara, T. Okuda, and S. Ichiba, *Bull. Chem. Soc. Japan* **61**, 4265 (1988).